Article

Discovery Medicine 2025; 37(199): 1651–1662
https://doi.org/10.24976/Discov.Med.202537199.144

Bafilomycin A1 Potentially Enhances Mesenchymal Stem Cell-derived Extracellular Vesicle Production in iPSC-MSC Cultures

Yuping Xiao[1,†], Weiyi Yuan[2,†], Shihong Chen[3], Gensheng Zhang[4], Qingling Fu[5,6], Zhijian Cai[7,8,*], Xinliang Lu[2,*]

[1]Department of Pediatrics, The Second Affiliated Hospital, Zhejiang University School of Medicine, 310058 Hangzhou, Zhejiang, China
[2]Department of Hepatobiliary and Pancreatic Surgery, Zhejiang Provincial Key Laboratory of Pancreatic Disease, The First Affiliated Hospital, Zhejiang University School of Medicine, 310006 Hangzhou, Zhejiang, China
[3]Department of Gastroenterology, The Second Affiliated Hospital and Yuying Children's Hospital of Wenzhou Medical University, 325027 Wenzhou, Zhejiang, China
[4]Department of Critical Care Medicine, The Second Affiliated Hospital, Zhejiang University School of Medicine, 310009 Hangzhou, Zhejiang, China
[5]Otorhinolaryngology Department, The First Affiliated Hospital, Sun Yat-sen University, 510080 Guangzhou, Guangdong, China
[6]Extracellular Vesicle Research and Clinical Translational Center, The First Affiliated Hospital, Sun Yat-sen University, 510080 Guangzhou, Guangdong, China
[7]Institute of Immunology, The Second Affiliated Hospital, Zhejiang University School of Medicine, 310058 Hangzhou, Zhejiang, China
[8]Department of Orthopaedics, The Second Affiliated Hospital, Zhejiang University School of Medicine, 310058 Hangzhou, Zhejiang, China
*Correspondence: caizj@zju.edu.cn (Zhijian Cai); xllu@zju.edu.cn (Xinliang Lu)
[†]These authors contributed equally.
Published: 20 August 2025

Background: Extracellular vesicles derived from stem cells (SC-EVs) show promise in regenerative medicine and inflammation resolution because of their low immunogenicity and translational potential. However, low SC-EV yields hinder their clinical scalability and therapeutic utility. Therefore, we aimed to enhance SC-EV production.

Methods: We explored strategies to enhance SC-EV production using Bafilomycin A1 (Baf-A1). The data are expressed as mean $\pm$ standard deviation (SD) values, and differences with $p < 0.05$ were considered significant.

Results: Baf-A1 increased the production of EVs from mesenchymal stem cells derived from induced pluripotent stem cells (iPSC-MSC-EVs) ($p < 0.01$). Mechanistically, Baf-A1 promotes iPSC-MSC-EV secretion while inhibiting their reuptake by the parent cells ($p < 0.0001$). Baf-A1 treatment preserved the gene and protein expression profiles of iPSC-MSC-EVs, maintaining their intrinsic biological properties and ensuring their reliability and safety for application. Furthermore, Baf-A1-treated induced pluripotent stem cell-derived mesenchymal stem cell extracellular vesicles (iPSC-MSC-EVs) demonstrated comparable therapeutic efficacy to untreated iPSC-MSC-EVs in acute liver injury (ALI) and inflammatory bowel disease (IBD) models, confirming their retained ability to promote tissue regeneration and anti-inflammation in these models.

Conclusions: These findings highlight Baf-A1 as a safe and potent modulator of iPSC-MSC-EV production, offering a strategy to overcome yield limitations and advance the clinical translation of iPSC-MSC-EVs in regenerative medicine and inflammatory disease therapy.

Keywords: iPSC-MSC-EVs; Bafilomycin A1; inflammatory disease; inhibitory reuptake

Introduction

Extracellular vesicles derived from stem cells (SC-EVs) are emerging as promising tools in regenerative medicine and inflammation resolution because they mimic stem cells' effects while avoiding the risks associated with cell therapy, such as immune rejection or tumor formation [1–3]. These vesicles play a critical role in metabolic regulation and intracellular communication, and their therapeutic potential has been demonstrated in various diseases, including cardiovascular diseases, kidney, liver, and neural injuries, and skin wounds [1,2,4–6]. The therapeutic effects of SC-EVs are attributed to their paracrine effects, particularly through the secretion of extracellular vesicles by stem cells, which influence a wide range of biological processes. However, the low yield of SC-EVs is a significant challenge that must be addressed to realize their clinical potential fully.

Bafilomycin A1 (Baf-A1), a potent inhibitor of Vacuolar H^+ ATPase (V-ATPase), a proton pump, plays a crucial role in acidifying intracellular compartments, such as lysosomes and endosomes [7]. This inhibition has significant

implications for both cellular function and the biogenesis and secretion of EVs. In a study, Baf-A1 was used to induce lysosomal dysfunction, and an increase in the secretion of autophagy-related proteins (such as microtubule-associated protein 1A/1B-light chain 3 (LC3)) in EVs was observed, indicating that Baf-A1 may regulate the cargo loading and release of EVs by altering the fate of multivesicular bodies (MVBs) [8]. A recent study demonstrated that Baf-A1 treatment results in an elevated release of EVs from mouse embryonic fibroblasts [9]. The increased release of EVs under Baf-A1 treatment could enhance the delivery of therapeutic cargoes or modulate immune responses. Whether the specific impact of Baf-A1 on SC-EVs' functionality remains an open question that requires further investigation.

SC-EVs have emerged as novel and promising therapeutic agents in regenerative medicine, particularly in tissue injury repair and inflammation resolution [10]. These nanoscale vesicles exhibit the capacity to mediate intercellular transfer of bioactive molecular cargo, encompassing proteins, lipids, and nucleic acids, thereby establishing their utility as a potent biological delivery platform for reprogramming cellular behavior and facilitating the healing process in damaged tissues. Studies have shown that SC-EVs have immunomodulatory properties and can significantly improve acute liver injury (ALI) [10]. In a mouse model of ALI induced by partial hepatectomy and ischemia-reperfusion injury, SC-EVs promoted regeneration of the remaining liver tissue, highlighting their critical role in liver regeneration [11]. In addition, SC-EVs ameliorated autoimmune hepatitis by modulating hepatic immune homeostasis and attenuating hepatic inflammation [12]. SC-EVs have also shown promising applications in drug-induced liver injury studies. For example, SC-EVs express liver-specific drug-metabolizing enzymes, synthesize albumin, and produce urea, making them useful in drug screening and hepatotoxicity testing [13]. In addition, SC-EVs have demonstrated anti-inflammatory efficacy in animal models of colitis, liver fibrosis, tendon repair, and atopic dermatitis [10]. Therefore, our current research focuses on increasing the yield of SC-EVs to improve their clinical applications.

The present study was designed to examine the pharmacological effects of Baf-A1 on EV production by mesenchymal stem cells derived from induced pluripotent stem cells (iPSC-MSCs). The objective of this study was to evaluate whether Baf-A1 could enhance EV yield by modulating the secretion and reuptake mechanisms without altering the gene or protein expression profiles of iPSC-MSCs. Additionally, we assessed the therapeutic efficacy of Baf-A1-treated iPSC-MSC-EVs in treating ALI and inflammatory bowel disease (IBD) compared to untreated EVs. These findings explore the potential of Baf-A1 as a strategy to optimize iPSC-MSC-EV production for therapeutic applications.

Materials and Methods

Mice

A total of 120 C57BL/6 mice (male, each weighing 21 $\pm$ 2 g, 6–8 weeks old) were obtained from SLAC Laboratory Animal Co. Ltd. (Shanghai, China). All mice were housed in a specific pathogen-free facility, and the Animal Care and Use Committee of Zhejiang University School of Medicine approved the experimental protocols (ethics number "ZJU20250369"). The animals were acclimatized for one week in an animal facility with a temperature of 23 $\pm$ 2 °C, a humidity of 35–60%, and a day-night alternation of 12 hours each. Euthanasia was performed by gradual displacement of chamber air with 100% CO_2 at a fill rate of 20% of the chamber volume per minute until a concentration $>$70% was achieved. Animals remained in the chamber for at least 10 minutes after respiratory arrest. Death was confirmed by absence of respiration, heartbeat, and bilateral fixed and dilated pupils.

Cell Culture

iPSC-MSCs were obtained from the American Type Culture Collection (ACS-5003™, ATCC, Manassas, VA, USA). These cells were cultured in iPSC-MSC culture medium (Dulbecco's modified Eagle's medium supplemented with 10% (v v^{-1}) fetal bovine serum (FBS), 1% penicillin/streptomycin, 1% L-Glutamax, 1% NEAA, 1 ng mL^{-1} bFGF, 10 ng mL^{-1} FGF, 55 µM β-mercaptoethanol). Mycoplasma testing and STR authentication were conducted to prevent cell contamination and ensure cell line stability.

iPSC-MSC-EVs Collection

iPSC-MSCs (2×10^4 cells mL^{-1}) were cultured in 10 mL of iPSC-MSC culture medium containing DMSO or 1 nM Baf-A1 for 10 days. During this period, 5 mL of iPSC-MSC culture medium with DMSO or 1 nM Baf-A1 (HY-100558, Medchemexpress, Shanghai, China) was added every 3 days. Culture supernatants were collected after 10 days for iPSC-MSC-EVs isolation.

Isolation of EVs

For the isolation of EVs, cell culture supernatants were subjected to centrifugation at 500 $\times$g for 10 minutes, 2000 $\times$g for 15 minutes, and 10,000 $\times$g for 30 minutes at 4 °C. Subsequently, the supernatants were filtered through 0.22 µm syringe filters (SLGPR33RB, Millipore, MA, USA) and collected in 35 mL ultracentrifuge tubes (Beckman Coulter, Brea, CA, USA). The EVs were then concentrated using ultracentrifugation with an SW32Ti rotor (L-90K with SW32Ti rotor, Beckman Coulter) at 100,000 $\times$g for 70 minutes at 4 °C. The protein content of the EVs was quantified using a bicinchoninic acid (BCA) assay protein assay kit (23223, Thermo Fisher Scientific, MA, USA).

Electron Microscopy

For negative staining of EVs, carbon films with a 200-mesh size were hydrophilized using a glow discharge instrument at a current of 15 mA for 25 seconds. An EV solution was then pipetted onto 200-mesh carbon-coated copper grids and allowed to sit at room temperature (RT) for 1 minute. Excess suspension was removed using filter paper, after which the EVs were negatively stained with a 2% solution of uranyl acetate at room temperature for another minute. Any remaining suspension was eliminated before the grids were left to air-dry. Images were captured using electron microscopy (Tecnai G2 Spirit, 120 kV, Thermo FEI, Hillsboro, OR, USA).

EV Size Distribution Analysis

The size distribution of EVs was measured using a Flow NanoAnalyzer (U30, NanoFCM, Xiamen, China). The instrument was calibrated for size distribution with a Silica Nanosphere Cocktail and for particle concentration with 250 nm SiNP beads. All particles detected were recorded over a 60-second interval. Samples were diluted in phosphate-buffered saline (PBS) at appropriate ratios and then analyzed under controlled flow conditions. The NanoFCM Professional 2.0 software (N30, NanoFCM, Xiamen, China) was used to analyze the size distribution and particle concentration data.

Western Blot

The lysates from iPSC-MSC-EVs were separated using SDS-PAGE and transferred onto PVDF membranes (03010040001, Millipore, MA, USA). Following a block with 5% BSA, the membranes were treated with primary antibodies overnight at 4 °C and subsequently with the appropriate secondary antibodies for 1 hour at room temperature. The membranes underwent three washes, each lasting 10 minutes, before being incubated with SuperSignal Chemiluminescent Substrate (Pierce, Dallas, TX, USA) and imaged using a Tanon 4500 Gel Imaging System (Tanon, Shanghai, China). The antibodies are detailed in **Supplementary Table 1**.

Flow Cytometric Analysis

To analyze EV amounts in cultured supernatants, EVs were incubated with 4-µm anti-cluster of differentiation 63 (CD63)-coated aldehyde sulfate latex beads (S37204, Thermo Fisher Scientific, MA, USA). Following incubation, the beads were washed and collected by centrifugation at 3500 ×g for 5 minutes at 4 °C. Subsequently, the beads were incubated with the corresponding fluorescence-conjugated primary antibodies in the dark at 4 °C for 20 minutes. After washing thrice with PBS, the samples were analyzed using an ACEA NovoCyteTM system (ACEA NovoCyteTM, Agilent Biosciences, Hangzhou, China). The antibodies used are listed in **Supplementary Table 1**.

MiRNA Sequencing Analysis

RNA purification, reverse transcription, library construction, and sequencing were performed at Shanghai Majorbio Bio-pharm Biotechnology Co., Ltd. (Shanghai, China) following the manufacturer's instructions (Illumina, San Diego, CA, USA). A total of 1 µg of RNA per sample was used as input material for the small RNA library. Sequencing libraries were generated using the QIAseq miRNA Library Kit (Qiagen, Dusseldorf, German) in accordance with the manufacturer's recommendations. The mapped small RNA tags were initially used to identify known miRNAs with the miRbase 2.0 database (http://www.mirbase.org/) as a reference. Subsequently, the remaining tags were aligned with the Rfam and Repbase databases to remove ribosomal RNA (rRNA), transfer RNA (tRNA), small nuclear RNA (snRNA), small nucleolar RNA (snoRNA), and other non-coding RNAs and repeats. The expression level of each miRNA was calculated using the transcripts per million reads (TPM) method. Differential expression analysis was conducted using DESeq2 or DEGseq. Differentially expressed genes (DEGs) with an absolute log2 fold change (|log2FC|) of at least 1 and a false discovery rate (FDR) of 0.05 or less (DESeq2) or 0.001 or less (DEGseq) were considered to be significantly differentially expressed.

Proteomics Analysis

Based on peptide quantification results, the peptides were analyzed by a VanquishNeo coupled with an Orbitrap Astral mass spectrometer (Thermo Fisher Scientific, MA, USA) at Majorbio BioPharm Technology Co.Ltd. (Shanghai, China) Briefly, the upAC FighThroughptu column (75 µm × 5.5 cm, Thermo Fisher Scientific, MA, USA) was used with solvent A (water with 296 ACN and 0.196 formic acid) and solvent B (water with 8096 ACN and 0.19b formic acid). The chromatography run time was set to 8 minutes. Data-independent acquisition (DiA) data were acquired using an Orbitrap Astralmass spectrometer operated in DiA mode. The mass spectrometry scanning range was 100–1700 m/z. Spectronaut software (Version 19, Biognosys, Zurich, Switzerland) was used to search the DiA raw data. The parameters are as follows: The peptide length range was set to 7–32; enzyme cutting site was typsin/P; the maximum missed cleavage site was 2; Carbamidometylation of cysteines as fixed modification, and addition of methionines and protein N-terminal acetylation as variable modifications; Protein false discovery rate (FDR) ≤0.01, Peptide FDR ≤0.01, Peptide Confdence >99%, extracted ion chromatogram (XIC) width ≤75 ppm. The protein quantification method was MaxLFQ.

Immunofluorescence Staining and Confocal Microscopy

iPSC-MSCs were plated on glass coverslips in 24-well plates. The cells were fixed in 4% paraformaldehyde for

30 minutes at room temperature (RT), permeabilized using 0.1% Triton X-100, blocked with 5% BSA in PBS for 1 hour, and then stained with specific antibodies. Nuclei were stained with DAPI, and the cell membrane was labeled with iFluor 488 phalloidin (Yeasen, Shanghai, China). Fluorescence was detected using an Olympus FV3000 laser scanning confocal microscope (OLYMPUS IX83-FV3000, Olympus, Japan). Images were analyzed with ImageJ software (NIH, Bethesda, USA). The antibodies used are listed in **Supplementary Table 1**.

D-GalN/LPS-mediated Acute Liver Injury

For ALI, mice were intraperitoneally injected with 400 mg kg^{-1} D-galactosamine (1772-03-8, Sigma-Aldrich, USA) and 50 µg kg^{-1} Escherichia coli 0111:B lipopolysaccharide [14] (93572-42-0, LPS, Sigma-Aldrich, USA) on day 0, and euthanized 24 h after injection. Histopathological assessment by Hematoxylin and Eosin (H&E) staining of the liver served as the primary criterion for validating the successful establishment of the liver injury model. Characteristic pathological features were quantitatively analyzed using the Ishak scoring system [15]. Mice with matched conditions were randomly assigned to four groups: "Blank" group, non-modeled, untreated controls; "PBS" group, disease-modeled mice treated with phosphate-buffered saline (PBS); "iPSC-MSC-EVs" group, disease-modeled mice receiving iPSC-MSC-EVs treatment; "Baf-A1-iPSC-MSC-EVs" group: disease-modeled mice receiving Baf-A1-iPSC-MSC-EVs treatment.

To assess the preventive effect of Baf-A1-iPSC-MSC-EVs, mice were pretreated with both types of iPSC-MSC-EVs on days -2 and -1. To assess the protective effect of Baf-A1-iPSC-MSC-EVs, mice were treated with both types of iPSC-MSC-EVs 6 h later after D-GalN/LPS injection.

DSS-induced Colitis

Mice were treated with 2.5% Dextran sulfate sodium salt (DSS, HY-116282C, MedChemExpress, Shanghai, China) for 7 days to induce acute colitis [14] and simultaneously received intravenous injections of PBS, iPSC-MSC-EVs or Baf-A1-iPSC-MSC-EVs every 2 days from day -1. Body weights were monitored every day. Mice were killed on day 8, and colons were collected to measure colon length. Mice with matched conditions were randomly assigned to four groups: "Blank" group, non-modeled, untreated controls; "PBS" group, disease-modeled mice treated with phosphate-buffered saline (PBS); "iPSC-MSC-EVs" group, disease-modeled mice receiving iPSC-MSC-EVs treatment; "Baf-A1-iPSC-MSC-EVs" group: disease-modeled mice receiving Baf-A1-iPSC-MSC-EVs treatment.

Histological Analysis

Mouse heart, liver, spleen, lung, kidney, and colon tissues were carefully excised, preserved in 4% paraformaldehyde, encased in paraffin, sliced, and stained with H&E. The resulting histological images were evaluated using ImageJ software.

Measurement of Cytokines

Enzyme-linked immunosorbent assay (ELISA) was utilized to quantify the levels of murine interleukin-6 (IL-6) and tumor necrosis factor (TNF) (provided by BioLegend, San Diego, CA, USA), as well as aspartate aminotransferase (AST) (C010-2-1, supplied by Nanjing Jiancheng, Nanjing, China) and ALT (C009-2-1, supplied by Nanjing Jiancheng, Nanjing, China), following the protocols specified by the manufacturer.

Cell Counting Kit-8 (CCK8) Assay

Cell proliferation was assessed using the CCK8 kit (C0037, Beyotime, Shanghai, China). After 72 hours of culturing with varying concentrations of Baf-A1, the absorbance at 450 nm was measured using a microplate reader (5250040, Thermo Scientific, Waltham, MA, USA). Each experiment was conducted in triplicate.

Statistical Analysis

Statistical comparisons were performed using Student's *t*-test for two-group analyses and one-way ANOVA with Tukey's post-hoc test for multiple-group comparisons. Data are presented as mean ± standard deviation and analyzed using GraphPad Prism 8.0 (GraphPad Software Inc., San Diego, CA, USA). *p*-values less than 0.05 were considered statistically significant.

Results

Baf-A1 Treatment Enhances iPSC-MSC-EV Production

To investigate whether Baf-A1 enhances iPSC-MSC-EV production, we first determined the optimal conditions for long-term iPSC-MSC culture with Baf-A1 without inducing cytotoxicity. The CCK8 assay indicated that iPSC-MSCs did not exhibit cytotoxicity when cultured at a concentration of 1 nM Baf-A1 rather than 2 nM for 3 days. Subsequently, we found that there was still no significant toxicity when cells were cultured continuously for 10 days at a concentration of 1 nM (Fig. 1a, $p < 0.05$). iPSC-MSC-EVs from iPSC with or without Baf-A1 treatment (Baf-A1-iPSC-MSC-EVs or Ctrl-iPSC-MSC-EVs) were harvested for subsequent analysis. As expected, Baf-A1 treatment significantly enhanced iPSC-MSC-EV output, as evidenced by an increase in the total protein amount of iPSC-MSC-EVs and $CD9^+$ iPSC-MSC-EV percentage in a semi-quantitative flow cytometry assay (Fig. 1b,c, $p < 0.01$). Enhanced production was further confirmed by the increased particle number of iPSC-MSC-EVs (Fig. 1d, $p < 0.001$). Therefore, Baf-A1 treatment led to an approximately 3-fold increase in iPSC-MSC-EV production. Subsequently, we

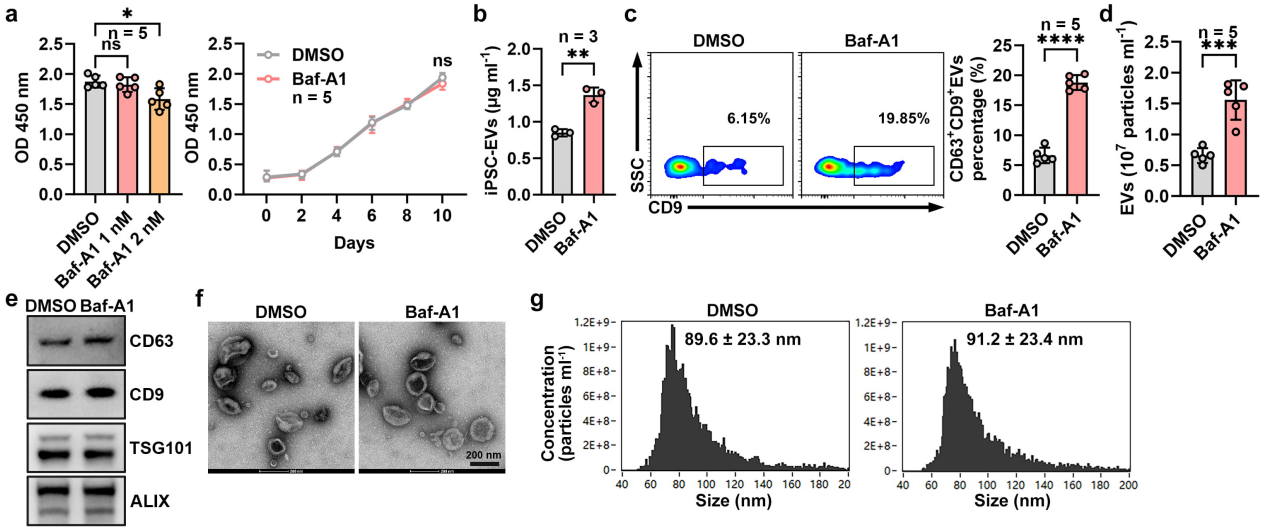

Fig. 1. Bafilomycin A1 (Baf-A1) treatment enhances EV from mesenchymal stem cells derived from induced pluripotent stem cells (iPSC-MSC-EV) production. (a) Cell Counting Kit-8 (CCK8) assay of iPSC-MSCs treated with DMSO or different concentrations of Baf-A1 for 3 days (left), CCK8 assay of iPSC-MSCs treated with 1 nM Baf-A1 for 10 days (right). (b) iPSC-MSC-EVs isolated from the culture supernatant were determined using the bicinchoninic acid (BCA) assay. (c) Flow cytometric analysis of anti-cluster of differentiation (CD63)-coated latex bead-captured $CD63^+CD9^+$ EVs. (d) Flow NanoAnalyzer analysis of Ctrl-iPSC-MSC-EVs and Baf-A1-iPSC-MSC-EVs particle numbers. (e) Western blot analysis of the indicated proteins in Ctrl-iPSC-MSC-EVs and Baf-A1-iPSC-MSC-EVs. (f) Morphology of Ctrl-iPSC-MSC-EVs and Baf-A1-iPSC-MSC-EVs was detected using transmission electron microscopy. Scale bars, 200 nm. (g) Size distribution of Ctrl-iPSC-MSC-EVs and Baf-A1-iPSC-MSC-EVs was analyzed using Flow NanoAnalyzer. ns, not significant; $*p < 0.05$; $**p < 0.01$; $***p < 0.001$; $****p < 0.0001$ (unpaired two-tailed Student's *t*-test; mean ± SD). n = 3, the data consists of three replicates. n = 5, the data consists of five replicates. TSG101, tumor susceptibility gene 101; ALIX, apoptosis-linked gene 2-interacting protein X.

found that the classical EV markers, CD63, CD9, tumor susceptibility gene 101 (TSG101), and apoptosis-linked gene 2-interacting protein X (ALIX), were comparable between Ctrl-iPSC-MSC-EVs and Baf-A1-iPSC-MSC-EVs (Fig. 1e). Furthermore, both EVs showed similar morphology and size distribution (Fig. 1f,g). These findings indicate that Baf-A1 significantly increased iPSC-MSC-EV production but did not alter the general characteristics of iPSC-MSC-EVs.

MicroRNA Sequencing Analysis of Baf-A1-treated iPSC-MSC-EVs

MicroRNAs (miRNAs) are key effector molecules in extracellular vesicles (EVs). To investigate whether Baf-A1 treatment alters the miRNA composition, we performed miRNA sequencing analysis of both Ctrl-iPSC-MSC-EVs and Baf-A1-iPSC-MSC-EVs. The results revealed that Ctrl-iPSC-MSC-EVs contained 6046 miRNAs, while Baf-A1-iPSC-MSC-EVs contained 6230 miRNAs. A violin plot analysis demonstrated that Baf-A1 treatment did not significantly perturb the overall miRNA expression profile in iPSC-MSC-EVs (Fig. 2a). However, further analysis showed that Baf-A1 treatment resulted in the 88 upregulated miRNAs and 43 downregulated miRNAs in iPSC-MSC-EVs (Fig. 2b,c).

To explore the functional implications of these differentially expressed miRNAs, we conducted Gene Ontology (GO) and Kyoto Encyclopedia of Genes and Genomes (KEGG) pathway enrichment analysis of their target genes. GO enrichment indicated that Baf-A1 treatment may significantly impact processes such as miRNA metabolism, osteoblast differentiation, leukocyte chemotaxis and differentiation, stress responses, and responses to xenobiotic stimuli (Fig. 2d). KEGG enrichment indicated that Baf-A1 treatment may significantly affect various cancer-related pathways, endocrine resistance, diabetic complications, cellular senescence, and the mitogen-activated protein kinase (MAPK) and transforming growth factor beta (TGF-β) signaling pathways (Fig. 2e). These findings suggest that Baf-A1 could influence cellular functions by modulating these biological processes, particularly in mechanisms related to cancer development, endocrine resistance, immune responses, and cellular stress responses. Altogether, Baf-A1 treatment alters the miRNA profile of iPSC-MSC-EVs to some extent but does not affect the miRNA content of iPSC-MSC-EVs associated with regenerative, anti-inflammatory, or antioxidant properties.

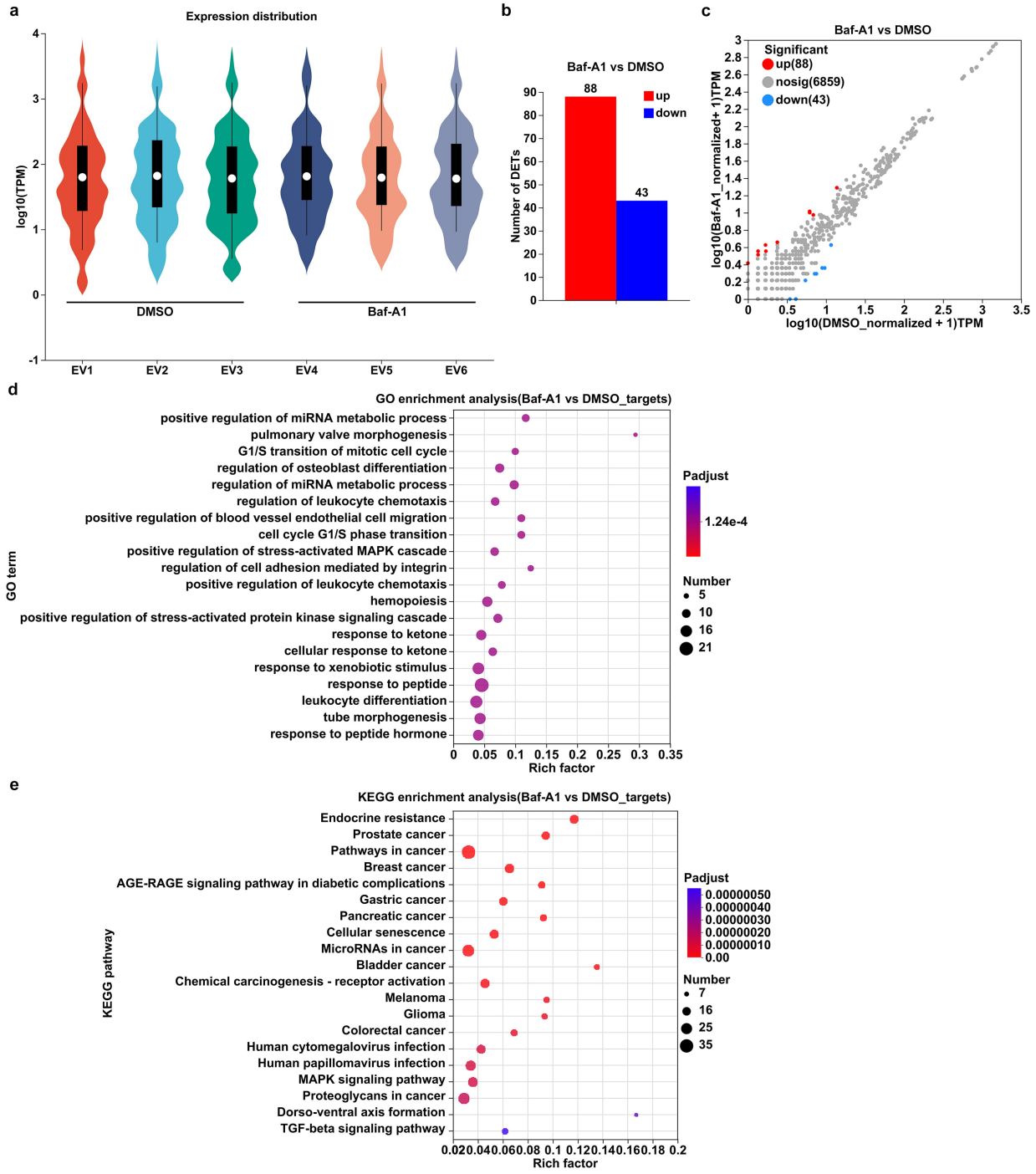

Fig. 2. MicroRNA sequencing analysis of Baf-A1-treated iPSC-MSC-EVs. (a) The violin plot showed miRNA expression in Ctrl-iPSC-MSC-EVs and Baf-A1-iPSC-MSC-EVs. (b) The number of differentially expressed miRNAs between Ctrl-iPSC-MSC-EVs and Baf-A1-iPSC-MSC-EVs. (c) The scatter plot showed the differentially expressed miRNAs in Ctrl-iPSC-MSC-EVs and Baf-A1-iPSC-MSC-EVs; red and blue dots indicate the upregulated and downregulated miRNAs, respectively. (d) Gene Ontology (GO) enrichment analysis of the target genes of differentially expressed miRNAs. (e) Kyoto Encyclopedia of Genes and Genomes (KEGG) enrichment analysis of the target genes of differentially expressed miRNAs.

Proteomics Analysis of Baf-A1-treated iPSC-MSC-EVs

Proteins also serve as essential effector molecules within EVs. To investigate whether Baf-A1 treatment alters the protein composition, we performed proteomics analysis on Ctrl-iPSC-MSC-EVs and Baf-A1-iPSC-MSC-EVs. The results revealed that Ctrl-iPSC-MSC-EVs contained 4512 proteins, while Baf-A1-iPSC-MSC-EVs con-

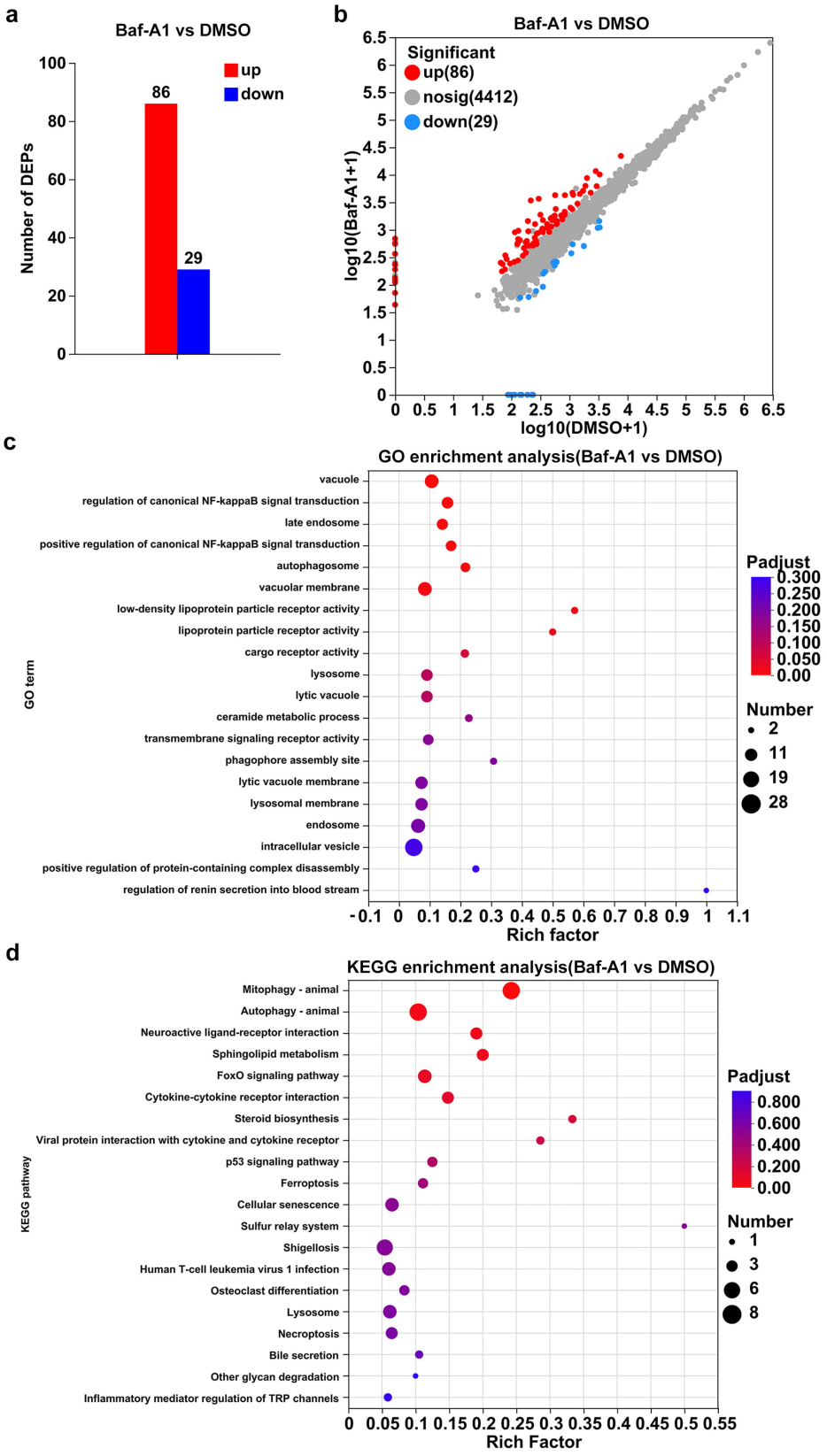

Fig. 3. Proteomics analysis of Baf-A1-treated iPSC-MSC-EVs. (a) The number of differentially expressed proteins between Ctrl-iPSC-MSC-EVs and Baf-A1-iPSC-MSC-EVs. (b) The scatter plot showed the differentially expressed proteins in Ctrl-iPSC-MSC-EVs and Baf-A1-iPSC-MSC-EVs; red and blue dots indicate the upregulated and downregulated proteins, respectively. (c) GO enrichment analysis of the differentially expressed proteins. (d) KEGG enrichment analysis of the differentially expressed proteins.

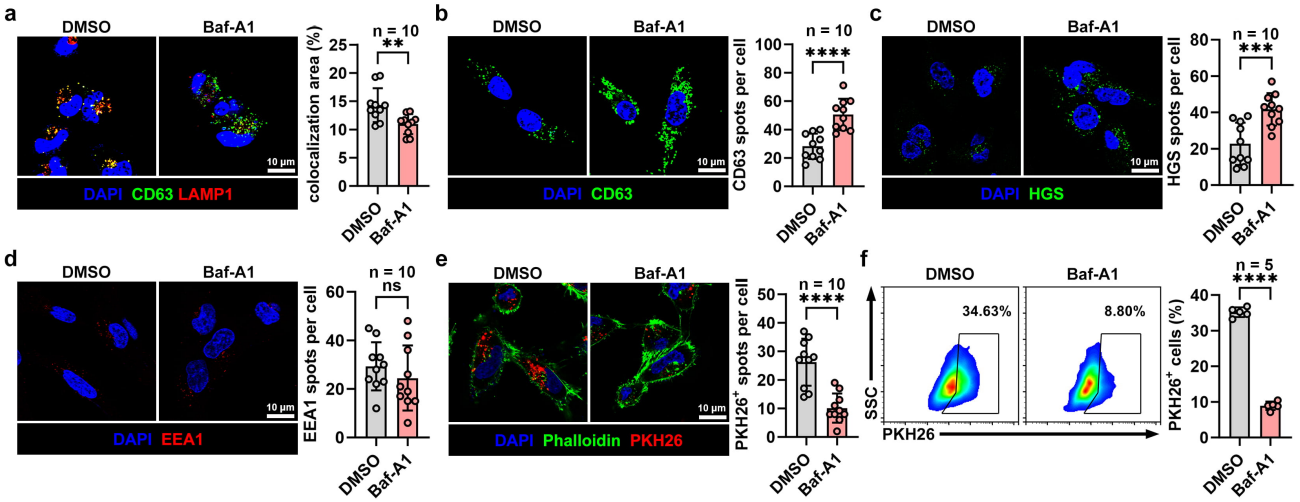

Fig. 4. Baf-A1 enhances iPSC-MSC-EV production by promoting EV secretion and reducing EV reuptake by iPSC-MSCs. (a) The colocalization of $CD63^+$ MVBs and $LAMP1^+$ lysosomes were detected with confocal microscopy. Scale bar, 10 μm. (b) The $CD63^+$ MVBs in iPSC-MSCs treated with DMSO or Baf-A1 were detected with confocal microscopy. Scale bar, 10 μm. (c) The hepatocyte growth factor-regulated tyrosine kinase substrate $(HGS)^+$ MVBs in iPSC-MSCs treated with DMSO or Baf-A1 were detected with confocal microscopy. Scale bar, 10 μm. (d) The $EEA1^+$ early endosomes in iPSC-MSCs treated with DMSO or Baf-A1 were detected with confocal microscopy. Scale bar, 10 μm. (e) The PKH26-labeled iPSC-MSC-EVs taken up by Phalloidin-labeled iPSC-MSCs treated with DMSO or Baf-A1 were detected with confocal microscopy. Scale bar, 10 μm. (f) The PKH26-labeled iPSC-MSC-EVs uptake by iPSC-MSCs treated with DMSO or Baf-A1 were examined with Flow cytometry. ns, not significant; $^{**}p < 0.01$; $^{***}p < 0.001$; $^{****}p < 0.0001$ (unpaired two-tailed Student's *t*-test; mean ± SD). n = 5; the data consists of five replicates. n = 10, the data consists of ten replicates.

tained 4514 proteins. Baf-A1 treatment resulted in the upregulation of 86 proteins and the downregulation of 29 proteins in iPSC-MSC-EVs (Fig. 3a,b). Then, we conducted GO and KEGG pathway enrichment analyses to explore the functional implications of these differentially expressed proteins. GO enrichment indicated that Baf-A1 treatment may significantly impact processes such as autophagy, the nuclear factor kappa B (NF-κB) signaling pathway, vesicle transport, and the disassembly of protein-containing complexes (Fig. 3c). KEGG enrichment indicated that Baf-A1 treatment may significantly impact autophagy (especially mitophagy), sphingolipid metabolism, cytokine interactions, and the forkhead box O (FoxO) and p53 signaling pathways (Fig. 3d). These findings suggest that Baf-A1 might influence cellular functions by modulating these biological processes, particularly in mechanisms related to autophagy, inflammation, and apoptosis. Again, these differentially expressed proteins were not associated with regenerative capacity, antioxidant properties, or immune modulation.

Baf-A1 Enhances iPSC-MSC-EV Production by Promoting EV Secretion and Reducing EV Reuptake by iPSC-MSCs

Then, we wondered how Baf-A1 increased iPSC-MSC-EV production. Baf-A1 has been demonstrated to prevent MVB and lysosome fusion, thereby increasing EV production [16]. As expected, Baf-A1 treatment markedly reduced the colocalization of $CD63^+$ MVBs and lysosomal-associated membrane protein 1 ($LAMP1^+$) lysosomes (Fig. 4a, $p < 0.01$). Correspondingly, $CD63^+$ and hepatocyte growth factor-regulated tyrosine kinase substrate $(HGS)^+$ MVBs were notably accumulated in Baf-A1-treated iPSC-MSCs (Fig. 4b,c, $p < 0.001$). In addition, Baf-A1 did not affect the origin of EVs because we detected a comparable number of $EEA1^+$ early endosomes in iPSC-MSCs with or without Baf-A1 treatment (Fig. 4d). These results indicate that Baf-A1 probably increases EV production by reducing lysosomal degradation of MVBs. We previously demonstrated that Baf-A1 can prevent EV reuptake by parental cells by inhibiting macropinocytosis of these cells [14]. Echoing that result, Baf-A1 also reduced the uptake of PKH26-labelled iPSC-MSC-EVs by iPSC-MSCs (Fig. 4e,f, $p < 0.0001$). Thus, these results suggest that increased EV secretion and decreased EV reuptake by iPSC-MSCs jointly contribute to the Baf-A1-mediated increase in iPSC-MSC-EV output.

Baf-A1 Treatment Does Not Affect iPSC-MSC-EVs' Protective Effects Against ALI

Since Baf-A1 effectively enhances iPSC-MSC-EV production, we wanted to know whether the primary functions of iPSC-MSC-EVs could be maintained. First, we evaluated the iPSC-MSC-EVs' abilities to regenerate tis-

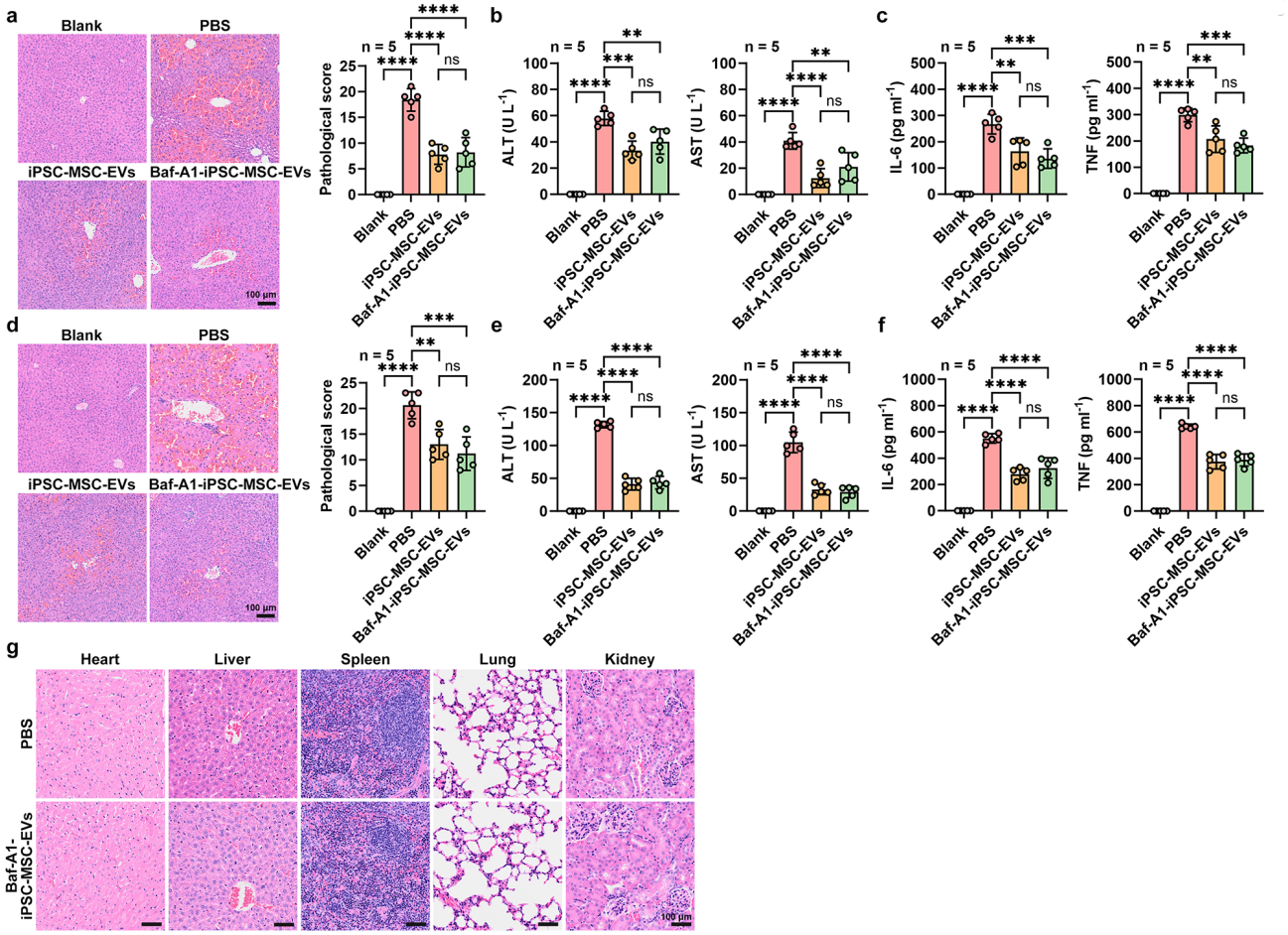

Fig. 5. Baf-A1-treated iPSC-MSC-EVs showed an ideal protective effect against acute liver injury (ALI). (a–c) ALI mice were induced by D-galactosamine (D-GalN) plus lipopolysaccharide (LPS) (D-GalN/LPS) treatment after intravenous injection of phosphate-buffered saline (PBS), iPSC-MSC-EVs and Baf-A1-iPSC-MSC-EVs. Blank was designated as the normal control. (a) Left, Hematoxylin and Eosin (H&E) staining of the liver tissues from these mice. Scale bar, 100 μm. Right, Pathological score. (b) Plasma alanine aminotransferase (ALT) and aspartate aminotransferase (AST) levels of these mice. (c) and enzyme-linked immunosorbent assay (ELISA) analysis of interleukin-6 (IL-6) and tumor necrosis factor (TNF) protein levels in the serum of these mice. (d–f) ALI mice were induced by D-GalN plus LPS (D-GalN/LPS) treatment and then intravenously injected with PBS, iPSC-MSC-EVs and Baf-A1-iPSC-MSC-EVs. Blank was designated as the normal control. (d) Left, H&E stained liver tissue sections of these mice. Scale bar, 100 μm. Right, Pathological score. (e) Plasma ALT and AST levels of these mice. (f) ELISA analysis of IL-6 and TNF protein levels in the serum of these mice. (g) H&E staining of the heart, liver, spleen, lungs, and kidneys from healthy mice treated only with PBS or Baf-A1-iPSC-MSC-EVs. Scale bar, 100 μm. ns, not significant; $^{**}p < 0.01$; $^{***}p < 0.001$; $^{****}p < 0.0001$ (one-way ANOVA followed by Tukey test; mean ± SD). n = 5, the data consists of five replicates.

sue using the mouse ALI model. Mice were pretreated with both types of iPSC-MSC-EVs for 2 days before induction of ALI, and Baf-A1-iPSC-MSC-EVs showed desirable preventive effects after assessment of liver histopathology, function and pro-inflammatory cytokine levels, which were comparable to Ctrl-iPSC-MSC-EVs (Fig. 5a–c, $p < 0.01$). In addition to the preventive effects, we tested iPSC-MSC-EVs' role in protecting ALI. When treated after ALI induction, both types of iPSC-MSC-EVs significantly and similarly alleviated ALI (Fig. 5d–f, $p < 0.001$). Furthermore, Baf-A1-treated iPSC-MSC-EVs did not cause any apparent histopathological damage to the major organs, including the heart, liver, spleen, lungs, and kidneys (Fig. 5g). Therefore, Baf-A1 treatment does not affect the abilities of iPSC-MSC-EVs in tissue regeneration.

Baf-A1 Treatment Does Not Affect iPSC-MSC-EVs' Protective Effects Against IBD

Since iPSC-MSC-EVs have been shown to exhibit significant anti-inflammatory effects, we investigated whether Baf-A1-iPSC-MSC-EVs retain their ability to suppress inflammation and alleviate the pathological progression of

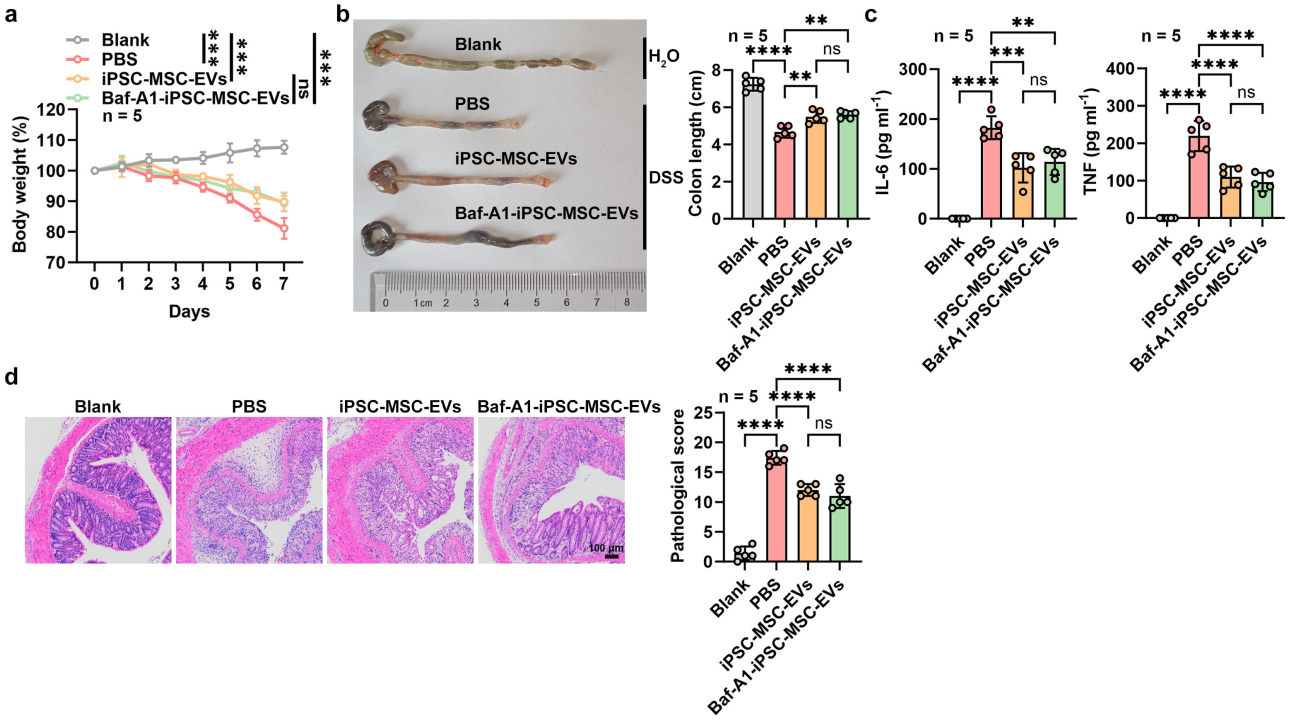

Fig. 6. Baf-A1-treated iPSC-MSC-EVs showed an ideal protective effect against inflammatory bowel disease (IBD). (a–d) Mice were treated with 2.5% Dextran sulfate sodium salt (DSS) for 7 days to induce acute colitis and simultaneously received intravenous injection of PBS, iPSC-MSC-EVs, or Baf-A1-iPSC-MSC-EVs every 2 days from day -1. (a) Body weight changes of these mice. (b) colon length of these mice. Scale bar, 100 μm. (c) Inflammatory cytokines in colon homogenates of these mice. (d) Left, H&E staining of colon tissue sections from these mice. Scale bar, 100 μm. Right, Pathological score. ns, not significant; $^{**}p < 0.01$; $^{***}p < 0.001$; $^{****}p < 0.0001$ (one-way ANOVA followed by Tukey test; mean ± SD). n = 5, the data consists of five replicates.

IBD. Our results showed that mice treated with iPSC-MSC-EVs or Baf-A1-iPSC-MSC-EVs exhibited similarly reduced weight loss and partial restoration of intestinal length (Fig. 6a,b, $p < 0.01$). Intestinal tissue homogenate supernatants from both groups of mice also contained identically lower inflammatory cytokines (Fig. 6c, $p < 0.01$). Moreover, H&E staining further confirmed that iPSC-MSC-EVs and Baf-A1-iPSC-MSC-EVs comparably improved intestinal tissue damage (Fig. 6d, $p < 0.0001$). Therefore, Baf-A1 treatment did not compromise the anti-inflammatory properties of iPSC-MSC-EVs and their therapeutic potential in IBD.

Discussion

This study establishes Baf-A1 as a potent and safe modulator capable of significantly enhancing iPSC-MSC-EV production, addressing a critical bottleneck in their translation into regenerative and anti-inflammatory therapies. The observed enhancement is driven by two key mechanisms: increased EV secretion through inhibition of MVB-lysosome fusion [16,17] and reduced EV reuptake by parent iPSC-MSCs via suppression of macropinocytosis [18]. These dual effects position Baf-A1 as a promising tool for optimizing EV-based therapies and advancing their translational potential in regenerative medicine and inflammation resolution [19]. Importantly, this yield enhancement strategy preserves the fundamental characteristics of iPSC-MSC-EVs, including their morphology, size distribution, and classical EV markers (CD63, CD9, TSG101, ALIX), while maintaining their therapeutic efficacy in both ALI and IBD models [20].

The comprehensive omics analyses revealed particularly insightful findings regarding cargo preservation. While Baf-A1 treatment induced minor changes in the miRNA (88 upregulated, 43 downregulated) and protein (86 upregulated, 29 downregulated) profiles, these alterations predominantly affected pathways unrelated to the core therapeutic functions of iPSC-MSC-EVs. The preserved expression of regenerative and anti-inflammatory mediators explains the maintained therapeutic efficacy observed in our disease models [21].

The clinical implications of this work are substantial. By overcoming the critical yield limitation without compromising quality or safety, Baf-A1 treatment represents a practical solution for scaling up iPSC-MSC-EV production to meet therapeutic demands. The absence of cytotoxicity at effective concentrations (1 nM) and the preserved organ histopathology in treated mice address key safety concerns for clinical translation. Furthermore, the retained therapeu-

tic potency at equivalent doses suggests that Baf-A1-iPSC-MSC-EVs could directly replace native iPSC-MSC-EVs in existing treatment protocols without requiring dosage adjustments.

While the study highlights Baf-A1's potential to enhance iPSC-MSC-EV production, several limitations and future directions warrant attention. Though not detrimental to the tested therapeutic outcomes, the minor changes in miRNA and protein profiles may impact iPSC-MSC-EVs' utility in other therapeutic contexts, such as cancer therapy or neurodegenerative disease treatment, where pathways like MAPK or p53 signaling are critical [22]. Future studies should evaluate the effects of Baf-A1-treated iPSC-MSC-EVs in specific contexts to refine the applicability of Baf-A1 across diverse therapeutic applications [23].

Integrating advanced production platforms, such as 3D culture methods and bioreactor systems, offers an ideal foundation for efficient EV production [24]. Leveraging this study's findings further to enhance the promoting effects of Baf-A1 in such systems is a promising area for future investigation. Ensuring cost-effectiveness and reproducibility in these platforms will be critical for advancing Baf-A1-modified iPSC-MSC-EVs toward clinical translation.

The work also opens several promising research directions: mechanistic studies to elucidate how Baf-A1 maintains selective cargo sorting during increased EV production, extensive animal studies to validate scalability, and exploration of Baf-A1's applicability to other therapeutically relevant EV sources [9]. Developing good manufacturing practice (GMP)-compatible protocols incorporating Baf-A1 treatment will be essential for clinical implementation.

In conclusion, this study demonstrates that Baf-A1 is an effective strategy to enhance iPSC-MSC-EV production, offering a solution to a longstanding challenge in EV-based therapeutics. Baf-A1 treatment advances iPSC-MSC-EVs toward clinical applications in regenerative medicine and inflammation management by maintaining the vesicles' therapeutic efficacy and safety profile. These findings not only emphasize the translational potential of Baf-A1 but also set the stage for broader exploration of pharmacological modulators in optimizing EV yield and functionality, accelerating the development of next-generation regenerative therapies [25].

Conclusion

The current study showed that Baf-A1 significantly increased iPSC-MSC-EV production but did not alter the general characteristics of iPSC-MSC-EVs. This is attributed to Baf-A1 promoting the secretion of IPSC-MSC-EV while reducing iPSC-MSC-EV reuptake. We found that Baf-A1-treated iPSC-MSC-EVs had equivalent protective effects against ALI and IBD at an equal dose compared with untreated iPSC-MSC-EVs. Therefore, adding Baf-A1 during iPSC-MSCs culture is likely a potential strategy to enhance iPSC-MSC-EVs' production.

Availability of Data and Materials

All data needed to evaluate the conclusions in the paper are presented in the main manuscript and the **Supplementary Table 1**.

Author Contributions

YPX, WYY, SHC performed various experiments; GSZ, QLF, ZJC, XLL designed the project and supervised the study; XLL and ZJC wrote the manuscript. All authors contributed to important editorial changes in the manuscript. All authors read and approved the final manuscript. All authors have participated sufficiently in the work and agreed to be accountable for all aspects of the work.

Ethics Approval and Consent to Participate

The Animal Care and Use Committee of Zhejiang University School of Medicine approved the experimental protocols (ethics number "ZJU20250369") involving mice.

Acknowledgment

We thank the Key Laboratory of Immunity and Inflammatory Diseases of Zhejiang Province for the support.

Funding

This work was supported by the National Key Research and Development Program of China (2022YFA1104900) and National Natural Science Foundation of China (82130053, 82000003, 31970845, 81971871).

Conflict of Interest

The authors declare no conflict of interest. Zhijian Cai is serving as one of the Editorial Board members of this journal. We declare that Zhijian Cai had no involvement in the review of this article and has no access to information regarding its review.

Supplementary Material

Supplementary material associated with this article can be found, in the online version, at https://doi.org/10.24976/Discov.Med.202537199.144.

References

[1] Karnas E, Dudek P, Zuba-Surma EK. Stem cell- derived extracellular vesicles as new tools in regenerative medicine - Immunomodulatory role and future perspectives. Frontiers in Immunology. 2023; 14: 1120175. https://doi.org/10.3389/fimmu.2023.1120175.

[2] Wang DR, Pan J. Extracellular vesicles: Emerged as a promising strategy for regenerative medicine. World Journal of Stem Cells. 2023; 15: 165–181. https://doi.org/10.4252/wjsc.v15.i4.165.

[3] Saneh H, Wanczyk H, Walker J, Finck C. Stem cell-derived extracellular vesicles: a potential intervention for Bronchopulmonary Dysplasia. Pediatric Research. 2025; 97: 497–509. https://doi.org/10.1038/s41390-024-03471-2.

[4] Petroni D, Fabbri C, Babboni S, Menichetti L, Basta G, Del Turco S. Extracellular Vesicles and Intercellular Communication: Challenges for In Vivo Molecular Imaging and Tracking. Pharmaceutics. 2023; 15: 1639. https://doi.org/10.3390/pharmaceutics15061639.

[5] Laura Francés J, Pagiatakis C, Di Mauro V, Climent M. Therapeutic Potential of EVs: Targeting Cardiovascular Diseases. Biomedicines. 2023; 11: 1907. https://doi.org/10.3390/biomedicines11071907.

[6] Park KS, Bandeira E, Shelke GV, Lässer C, Lötvall J. Enhancement of therapeutic potential of mesenchymal stem cell-derived extracellular vesicles. Stem Cell Research & Therapy. 2019; 10: 288. https://doi.org/10.1186/s13287-019-1398-3.

[7] Li W, Kawaguchi K, Tanaka S, He C, Maeshima Y, Suzuki E, *et al*. Cellular senescence triggers intracellular acidification and lysosomal pH alkalinized via ATP6AP2 attenuation in breast cancer cells. Communications Biology. 2023; 6: 1147. https://doi.org/10.1038/s42003-023-05433-6.

[8] Dixson AC, Dawson TR, Di Vizio D, Weaver AM. Context-specific regulation of extracellular vesicle biogenesis and cargo selection. Nature Reviews. Molecular Cell Biology. 2023; 24: 454–476. https://doi.org/10.1038/s41580-023-00576-0.

[9] Liang W, Sagar S, Ravindran R, Najor RH, Quiles JM, Chi L, *et al*. Mitochondria are secreted in extracellular vesicles when lysosomal function is impaired. Nature Communications. 2023; 14: 5031. https://doi.org/10.1038/s41467-023-40680-5.

[10] Barreca MM, Cancemi P, Geraci F. Mesenchymal and Induced Pluripotent Stem Cells-Derived Extracellular Vesicles: The New Frontier for Regenerative Medicine? Cells. 2020; 9: 1163. https://doi.org/10.3390/cells9051163.

[11] Zhang L, Pu K, Liu X, Bae SDW, Nguyen R, Bai S, *et al*. The Application of Induced Pluripotent Stem Cells Against Liver Diseases: An Update and a Review. Frontiers in Medicine. 2021; 8: 644594. https://doi.org/10.3389/fmed.2021.644594.

[12] Muñoz-Hernández R, Rojas Á, Gato S, Gallego J, Gil-Gómez A, Castro MJ, *et al*. Extracellular Vesicles as Biomarkers in Liver Disease. International Journal of Molecular Sciences. 2022; 23: 16217. https://doi.org/10.3390/ijms232416217.

[13] Carberry CK, Ferguson SS, Beltran AS, Fry RC, Rager JE. Using liver models generated from human-induced pluripotent stem cells (iPSCs) for evaluating chemical-induced modifications and disease across liver developmental stages. Toxicology in Vitro: an International Journal Published in Association with BIBRA. 2022; 83: 105412. https://doi.org/10.1016/j.tiv.2022.105412.

[14] Lu X, Song Z, Hao J, Kong X, Yuan W, Shen Y, *et al*. Proton pump inhibitors enhance macropinocytosis-mediated extracellular vesicle endocytosis by inducing membrane v-ATPase assembly. Journal of Extracellular Vesicles. 2024; 13: e12426. https://doi.org/10.1002/jev2.12426.

[15] Ishak K, Baptista A, Bianchi L, Callea F, De Groote J, Gudat F, *et al*. Histological grading and staging of chronic hepatitis. Journal of Hepatology. 1995; 22: 696–699. https://doi.org/10.1016/0168-8278(95)80226-6.

[16] Villarroya-Beltri C, Baixauli F, Mittelbrunn M, Fernández-Delgado I, Torralba D, Moreno-Gonzalo O, *et al*. ISGylation controls exosome secretion by promoting lysosomal degradation of MVB proteins. Nature Communications. 2016; 7: 13588. https://doi.org/10.1038/ncomms13588.

[17] Sinha S, Hoshino D, Hong NH, Kirkbride KC, Grega-Larson NE, Seiki M, *et al*. Cortactin promotes exosome secretion by controlling branched actin dynamics. The Journal of Cell Biology. 2016; 214: 197–213. https://doi.org/10.1083/jcb.201601025.

[18] Tian T, Zhu YL, Zhou YY, Liang GF, Wang YY, Hu FH, *et al*. Exosome uptake through clathrin-mediated endocytosis and macropinocytosis and mediating miR-21 delivery. The Journal of Biological Chemistry. 2014; 289: 22258–22267. https://doi.org/10.1074/jbc.M114.588046.

[19] Phinney DG, Pittenger MF. Concise Review: MSC-Derived Exosomes for Cell-Free Therapy. Stem Cells (Dayton, Ohio). 2017; 35: 851–858. https://doi.org/10.1002/stem.2575.

[20] Song L, Tang S, Han X, Jiang Z, Dong L, Liu C, *et al*. KIBRA controls exosome secretion via inhibiting the proteasomal degradation of Rab27a. Nature Communications. 2019; 10: 1639. https://doi.org/10.1038/s41467-019-09720-x.

[21] Reza-Zaldivar EE, Hernández-Sapiéns MA, Gutiérrez-Mercado YK, Sandoval-Ávila S, Gomez-Pinedo U, Márquez-Aguirre AL, *et al*. Mesenchymal stem cell-derived exosomes promote neurogenesis and cognitive function recovery in a mouse model of Alzheimer's disease. Neural Regeneration Research. 2019; 14: 1626–1634. https://doi.org/10.4103/1673-5374.255978.

[22] Kalluri R, LeBleu VS. The biology, function, and biomedical applications of exosomes. Science (New York, N.Y.). 2020; 367: eaau6977. https://doi.org/10.1126/science.aau6977.

[23] Zhang Y, Liu Y, Liu H, Tang WH. Exosomes: biogenesis, biologic function and clinical potential. Cell & Bioscience. 2019; 9: 19. https://doi.org/10.1186/s13578-019-0282-2.

[24] Dos Santos NCD, Bruzadelle-Vieira P, de Cássia Noronha N, Mizukami-Martins A, Orellana MD, Bentley MVLB, *et al*. Transitioning from static to suspension culture system for large-scale production of xeno-free extracellular vesicles derived from mesenchymal stromal cells. Biotechnology Progress. 2024; 40: e3419. https://doi.org/10.1002/btpr.3419.

[25] van Niel G, D'Angelo G, Raposo G. Shedding light on the cell biology of extracellular vesicles. Nature Reviews. Molecular Cell Biology. 2018; 19: 213–228. https://doi.org/10.1038/nrm.2017.125.